BRAIN
ORIGINAL ARTICLE

Cerebrovascular insulin receptors are defective in Alzheimer's disease

Manon Leclerc,[1,2,3] Philippe Bourassa,[1,2] Cyntia Tremblay,[2] Vicky Caron,[1,2] Camille Sugère,[2] Vincent Emond,[2] David A. Bennett[4] and Frédéric Calon[1,2,3]

See Hughes and Craft (https://doi.org/10.1093/brain/awac433) for a scientific commentary on this article.

Central response to insulin is suspected to be defective in Alzheimer's disease. As most insulin is secreted in the bloodstream by the pancreas, its capacity to regulate brain functions must, at least partly, be mediated through the cerebral vasculature. However, how insulin interacts with the blood–brain barrier and whether alterations of this interaction could contribute to Alzheimer's disease pathophysiology both remain poorly defined.

Here, we show that human and murine cerebral insulin receptors (INSRs), particularly the long isoform INSRα-B, are concentrated in microvessels rather than in the parenchyma. Vascular concentrations of INSRα-B were lower in the parietal cortex of subjects diagnosed with Alzheimer's disease, positively correlating with cognitive scores, leading to a shift towards a higher INSRα-A/B ratio, consistent with cerebrovascular insulin resistance in the Alzheimer's disease brain. Vascular INSRα was inversely correlated with amyloid-β plaques and β-site APP cleaving enzyme 1, but positively correlated with insulin-degrading enzyme, neprilysin and P-glycoprotein. Using brain cerebral intracarotid perfusion, we found that the transport rate of insulin across the blood–brain barrier remained very low (<0.03 µl/g·s) and was not inhibited by an insulin receptor antagonist. However, intracarotid perfusion of insulin induced the phosphorylation of INSRβ that was restricted to microvessels. Such an activation of vascular insulin receptor was blunted in 3xTg-AD mice, suggesting that Alzheimer's disease neuropathology induces insulin resistance at the level of the blood–brain barrier.

Overall, the present data in post-mortem Alzheimer's disease brains and an animal model of Alzheimer's disease indicate that defects in the insulin receptor localized at the blood–brain barrier strongly contribute to brain insulin resistance in Alzheimer's disease, in association with β-amyloid pathology.

1 Faculté de Pharmacie, Université Laval, Québec, QC G1V 0A6, Canada
2 Axe Neurosciences, Centre de Recherche du CHU de Québec-Université Laval, Quebec, QC G1V 4G2, Canada
3 Institut sur la Nutrition et les Aliments Fonctionnels (INAF), Québec, QC G1V 0A6, Canada
4 Rush Alzheimer's Disease Center, Rush University Medical Center, Chicago, IL 60612, USA

Correspondence to: Frédéric Calon
Centre de recherche du CHU de Québec – Université Laval
2705, Boulevard Laurier, Room T2-67
Québec, QC, G1V 4G2, Canada
E-mail: Frederic.Calon@crchul.ulaval.ca

Keywords: blood–brain barrier; insulin receptor; Alzheimer's disease; insulin resistance

Introduction

The human brain is sensitive to insulin, a hormone essential to life that is also at the heart of the pathophysiology and treatment of diabetes.[1,2] The scientific literature is replete with studies in humans and other species reporting the effects of insulin on memory, cerebral blood flow, eating behaviour and regulation of whole-body metabolism, supporting a therapeutic potential in brain-dependent

Received March 31, 2022. Revised June 24, 2022. Accepted August 12, 2022. Advance access publication October 25, 2022

metabolic disorders.[3–6] Although local synthesis has been detected, most insulin exercising an effect on the brain circulates in the blood after being produced by the pancreas.[7,8] The blood–brain barrier (BBB) is a major interface between the blood and brain, controlling access to cerebral tissues. Therefore, to exert an effect in the CNS, circulating insulin must first interact with its insulin receptor (INSR) located on brain capillary endothelial cells (BCEC) forming the BBB.[8–11]

INSR is a disulphide-linked homodimer $(\alpha\beta)_2$ that structurally and genetically belongs to the class II of receptor tyrosine kinases. Alternative splicing produces two isoforms of the α-chain: the short A isoform (INSRα-A) truncated by 12 amino acids (exon 11) and the long B isoform (INSRα-B).[12–15] The regulation of this alternative splicing is not fully elucidated but appears to be tissue-specific.[12] Binding of an agonist to the extracellular α-chain triggers autophosphorylation of the transmembrane β-chain, which contains multiple phosphorylation sites leading to the activation of INSR and downstream signalling pathways.

Beside classical amyloid-β (Aβ) and tau pathologies, Alzheimer's disease is characterized by defective brain uptake of glucose and impaired response to insulin.[4,5,16–19] The most compelling evidence comes from post-mortem indexes of brain insulin resistance, such as changes in INSR or IRS1 phosphorylation status shown to be associated with cognitive impairment.[20,21] Insulin administration in animals is reported to improve memory function, including in mouse models of Alzheimer's disease.[22,23] Several small clinical trials using intranasal delivery to avoid the hypoglycaemic effect of systemically injected insulin have reported benefits to memory scores in cognitively impaired adults.[6,24,25] However, recent larger clinical trials produced unclear results.[6,25–27] Still, increasing insulin sensitivity in the brain remains a promising avenue and a wide range of repurposed diabetes drugs are in ongoing clinical trials for Alzheimer's disease, including metformin, thiazolidinediones and glucagon-like peptide 1 (GLP-1) analogues.[6,28,29]

Whereas cerebral insulin resistance is often assumed to be restricted to neurons in Alzheimer's disease,[30–32] it is supported by limited immunohistochemical (IHC) evidence.[33,34] Most initial studies on the distribution of brain INSR used macroscopic techniques.[35–39] However, recent single-cell transcriptomic analyses indicate that the mRNA transcript encoded by the *INSR* gene is found in higher concentrations in endothelial cells in the mouse and human brain.[40–42] Accordingly, a growing number of studies are showing that INSR located in the cerebral vasculature plays a key role in the action of insulin on the brain.[11,43,44] Based on the current understanding, INSR at the BBB binds circulating insulin to either act (i) as a classic receptor to trigger cell-signalling pathways within BCEC; or (ii) as a transporter to ferry an insulin molecule into the brain parenchyma.[45–49] Therefore, it remains unclear whether the same INSR protein can exert both roles.[8,50–52]

Given this large set of clinical and preclinical data showing a primary role of insulin on brain function, we aimed to determine how circulating insulin interacts with the BBB INSR and whether the latter is defective in Alzheimer's disease. We first sought to determine INSR levels in microvascular extracts from both mouse and human brain samples relative to brain parenchyma. To probe for changes in Alzheimer's disease, we used microvessel extracts of parietal cortex from participants in the Religious Orders Study who underwent detailed clinical and neuropsychological evaluations.[53–55] Associations with clinical and biochemical data were assessed, including BBB transporters and receptors putatively involved in Aβ transport. To directly investigate the response of brain INSR to circulating insulin, we performed intracarotid insulin perfusion and found that INSR activation is localized at the BBB, where it is impaired by Aβ and tau pathologies in a mouse model of Alzheimer's disease at different ages.

Materials and methods

Human samples: Religious Orders Study

Parietal cortex samples were obtained from participants in the Religious Orders Study (ROS), a longitudinal clinical and pathological study of ageing and dementia.[53–55] Each participant enrolled without known dementia and agreed to an annual detailed clinical evaluation and brain donation at death. The study was approved by an Institutional Review Board of Rush University Medical Center. All participants signed an informed consent, an Anatomic Gift Act for brain donation and a repository consent allowing their data and biospecimens to be shared. A total of 21 cognitive performance tests were administered, of which 19 were used to create a global measure of cognition and five cognitive domains: episodic, semantic, working memory, perceptual speed and visuospatial ability.[56,57] Participants received a clinical diagnosis of Alzheimer's dementia, mild cognitive impairment (MCI) or no cognitive impairment (NCI) ($n = 20$ for each group) at the time of death by a neurologist, blinded to all post-mortem data, as previously described.[56,58,59] In addition, current prescription medication usage in the last 2 weeks before each evaluation were available, such as antihypertensive and diabetes medications.[60,61] The neuropathological diagnosis is based on the ABC scoring method found in the revised National Institute of Aging–Alzheimer's Association (NIA-AA) guidelines for the neuropathological diagnosis of Alzheimer's disease.[62] Four levels of Alzheimer's disease neuropathological changes (not, low, intermediate or high) were determined using: (i) Thal score assessing phases of Aβ plaque accumulation[63]; (ii) Braak score assessing neurofibrillary tangle pathology[64]; and (iii) CERAD (Consortium to Establish a Registry for Alzheimer's Disease) score assessing neuritic plaque pathology.[65] Individuals classified as 'Controls' had no or a low level of Alzheimer's disease neuropathological changes while those classified as 'AD' included participants with intermediate or high levels of Alzheimer's disease neuropathological changes.[55] Neuritic plaques and neurofibrillary tangles in the parietal cortex were counted following Bielschowsky silver impregnation, as previously described.[66] As previously described,[55,67,68] soluble and insoluble levels of $A\beta_{40}$ and $A\beta_{42}$ were also assessed in homogenates and microvascular extracts of parietal cortex. See Supplementary Table 1 for the characteristics of the cohort.

Animals

All animals had free access to laboratory food and water and were maintained under a 12-h light–dark cycle at 22°C. The 3xTg-AD mouse model of genetically induced Alzheimer's dementia-like neuropathology is a widely used model that progressively develops both Aβ deposits and neurofibrillary tangles (τ pathology) as well as cognitive deficits, due to the expression of three mutant genes: β-amyloid precursors protein (APP_{swe}), presenilin-1 ($PS1_{MA146V}$) and tau (tau_{P301L}).[69,70] It fully develops neuropathological and behavioural changes ~12 months of age.[71–73] Although the 3xTg-AD mouse is considered a model of modest overproduction of Aβ and tau, signs of defects in Aβ clearance have been detected at older ages.[22,74,75] Previous studies showed that 3xTg-AD mice also display metabolic disorders, such as glucose intolerance or impaired insulin sensitivity, aggravated by old age and

high-fat diets.[22,23,70,73,76–78] Brain Aβ concentrations in this model decrease after insulin administration.[22,79] Here, they were compared with non-transgenic (non-Tg) littermates with the same genetic background (C57Bl6/129SvJ). All groups of 3xTg-AD and non-Tg mice were randomly assigned to experimental conditions. For all experiments 3xTg-AD mice between 6 and 18 months were used for microvessel comparisons (42 males and 34 females) and for intracarotid *in situ* cerebral perfusion (ICSP, 35 males and 30 females). In addition, 6-month-old C57Bl/6 mice (11 males and 13 females) were used for insulin stimulation experiments (Supplementary Fig. 1), and for insulin transport quantification 15-week-old males Balb/c ($n = 22$), C57Bl/6 mice ($n = 7$), 13.5-month-old non-Tg ($n = 20$) and 3xTg-AD ($n = 21$) female mice were used.

Isolation of brain microvessels

Human brain microvessels were extracted following the procedure described previously.[55] Following a series of centrifugation steps, including a density gradient centrifugation with dextran and a filtration (20-µm nylon filter), two fractions were obtained: one enriched in cerebral microvessels, the other consisting of microvessel-depleted parenchymal cell populations. Examples of the efficiency of the separation are shown in Fig. 1, using immunodetection of endothelial and neuronal markers.[55] Proteins of both fractions were extracted using a lysis buffer (150 mM NaCl, 10 mM NaH_2PO_4, 1 mM EDTA, 1% Triton X-100, 0.5% SDS and 0.5% deoxycholate) containing the same protease and phosphatase inhibitors cocktails (Bimake), and supernatants were kept for western immunoblotting analyses. Brain microvessels from mice were generated with a similar procedure reported in previous work[54,55,80] after an intracardially perfusion with phosphate saline buffer containing a cocktail of protease inhibitors (SIGMAFAST™ Protease Inhibitor Tablets #S8820) and phosphatase inhibitors (1 mM sodium pyrophosphate and 50 mM sodium fluoride) under deep anaesthesia with ketamine/xylazine intraperitoneal (300/30 mg/kg). A scheme is shown in Supplementary Fig. 1.

Acute exposition of the BBB to insulin using intracarotid *in situ* cerebral perfusion

The *in situ* cerebral perfusion (ISCP) technique consists in a direct cerebral infusion of a labelled compound at the BBB through the right common carotid artery.[81] Briefly, mice were anaesthetized by intraperitoneal injection of a mixture of ketamine/xylazine intraperitoneally (140/8 mg/kg). The right external and the right common carotid artery were ligated, and the common carotid artery was catheterized with polyethylene tubing (0.30 × 0.70 mm) filled with heparin (25 IU/ml). The syringe containing the perfusion fluid was placed in an infusion pump and connected to the catheter. The thorax was opened, the heart cut and perfusion started immediately. The perfusion fluid contained bicarbonate buffered physiologic saline containing 128 mM NaCl, 24 mM $NaHCO_3$, 4.2 mM KCl, 2.4 mM NaH_2PO_4, 1.5 mM $CaCl_2$, 0.9 mM $MgCl_2$ and 9 mM D-glucose. The solution was gassed with 95% O_2–5% CO_2 for pH control (7.4), filtrated (0.20 µm) and used at 37°C. For radiolabelled insulin transport experiment mice were perfused with 0.1 nM of ^{125}I-insulin, 0.3 µCi/ml of ^{3}H-sucrose as a vascular marker and 20 nM S961 for competition. The physiological buffer was supplemented with 0.25% bovine serum albumin (BSA) and the perfusion lasted 120 s at 1.25 ml/min. For insulin stimulation studies, 6-month-old C57Bl6 and 16-month-old non-Tg and 3xTg-AD mice were perfused for 120 s, at 2.5 ml/min, with insulin (100 or 350 nM) or saline.

Immunofluorescence analysis of isolated human microvessels

The method was similar to previous publications.[54,55] Both vascular and microvessel-depleted extracts on glass side were fixed using a 4% paraformaldehyde solution in phosphate buffer saline (PBS) for 20 min at room temperature (RT) and then blocked with a 10% normal horse serum and 0.1% Triton X-100 solution in PBS or commercial TrueBlack® Background Suppressor and Blocking Buffer (Biotium) for 1 h at RT. For Aβ immunolabeling, an additional pretreatment with 90% formic acid during 10 min was performed between the fixation and blocking steps. Following an incubation overnight at 4°C with primary antibodies diluted in a 1% NHS and 0.05% Triton X-100 solution in PBS, or TrueBlack® Blocking Buffer (Biotium), vascular and microvessel-depleted extracts were incubated with secondary antibodies diluted in the same solution as the primary antibodies during 1 h at RT. Primary and secondary antibodies are listed in Supplementary Table 2. Cell nuclei were counterstained with DAPI (Thermo Fisher Scientific, 0.02% in PBS) and slides were mounted with Mowiol mounting medium or Prolong™ Diamond antifade (Thermo Fisher Scientific). If needed, slides were incubated with TrueBlack® Plus (Biotium) and TrueView® (Vector Laboratories) to decrease autofluorescence and background. Between each step, three washes of 5 min in PBS were performed.

Images were taken using a fluorescence microscope (EVOS Fl Autoimaging system, Thermo Fisher Scientific) at magnification ×20–40 or a laser scanning confocal microscope (Olympus IX81, FV1000) with sequential scanning acquisition using optimal z-separation at a magnification of ×20.

Western blot

For western immunoblotting, proteins from the vascular fraction were extracted and a protein quantification was done using bicinchoninic acid assays (Thermo Fisher Scientific). Protein homogenates from human and murine brain microvascular extracts were added to Laemmli's loading buffer and samples were heated for 10 minutes at 70°C (human and 3xTg-AD samples) or not (samples from insulin stimulation studies). Equal amounts of proteins per sample (4–8 µg) were resolved on a sodium dodecyl sulphate–polyacrylamide gel electrophoresis (SDS–PAGE) 8% acrylamide. All samples, loaded in a random order, were run on the same immunoblot experiment for quantification.

Proteins were electroblotted on PVDF membranes, which were then blocked during 1 h at RT with Superblock™ in PBS blocking buffer (Thermo Fisher Scientific) or PBS containing 0.1% Tween 20 and 3% BSA. If needed, membranes were stained with No-Stain™ protein labelling reagent (Thermo Fisher Scientific) to assess a similar protein load in the samples. Membranes were then incubated overnight at 4°C with primary antibodies (all listed in Supplementary Table 2). Membranes were then washed three times with PBS containing 0.1% Tween 20 and incubated during 1 h at RT with the secondary antibody in PBS containing 0.1% Tween 20 and 1% BSA. Membranes were probed with chemiluminescence reagent (Luminata Forte Western horseradish peroxidase substrate, Millipore) and imaged using the myECL imager system (Thermo Fisher Scientific) or the Amersham Imager 680 (GE Healthcare Bio-Sciences). Densitometric analysis was performed using the Image Lab™ Software. Uncropped gels of immunoblotting experiments conducted with human samples are shown in Supplementary Fig. 2.

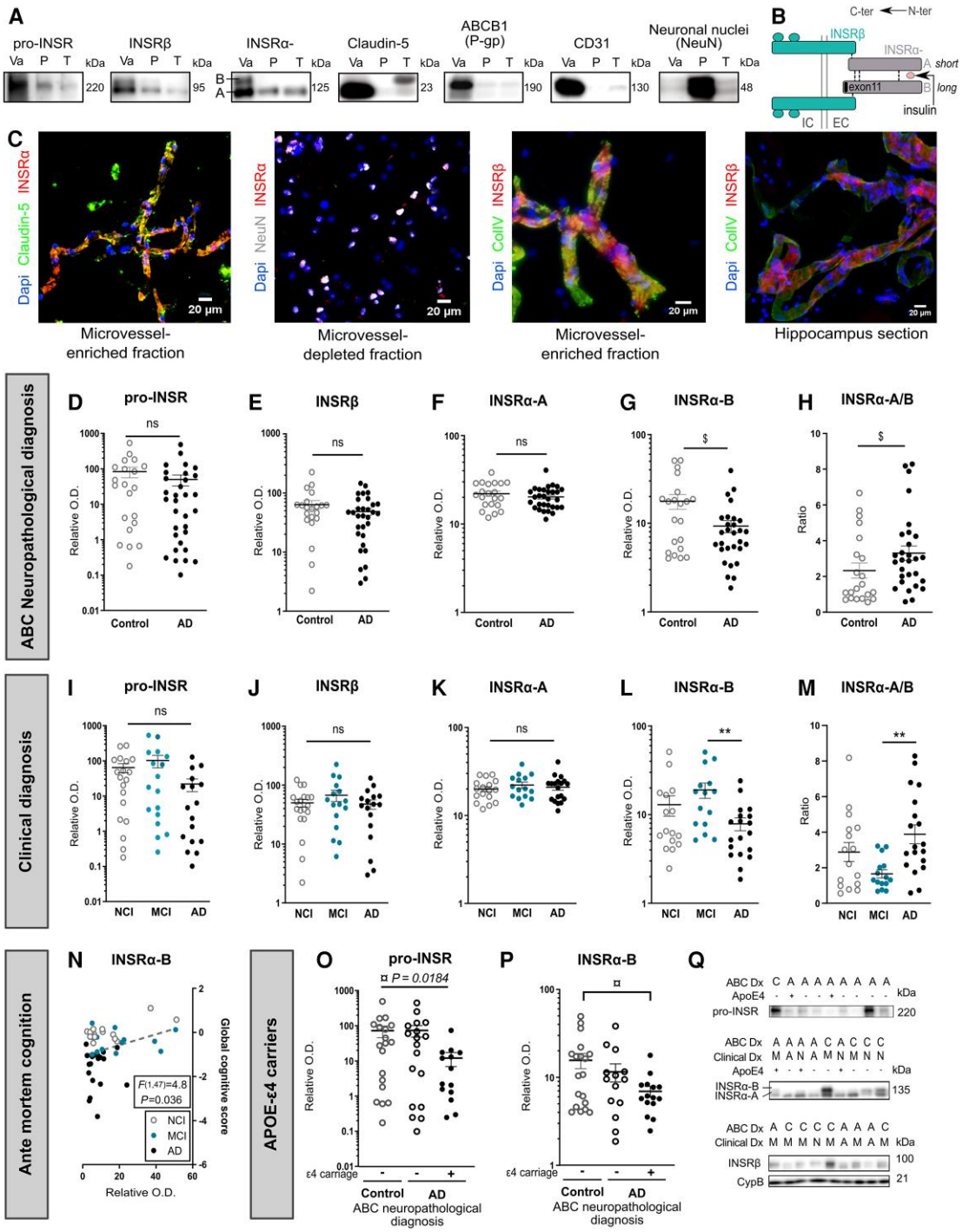

Figure 1 INSRα-B levels are reduced in Alzheimer's disease, correlating with cognitive dysfunction. (**A**) Pro-INSR, INSRα and INSRβ are enriched in vascular fractions from the parietal cortex, along with endothelial markers claudin-5, ABCB1(P-gp) and CD31, whereas NeuN, a neuronal marker, is rather concentrated in the microvessel-depleted parenchymal fraction. (**B**) Schematic representation of the transmembrane INSR: the extracellular α chain binds circulating insulin and the intracellular β chain acts as a primary effector of insulin signaling pathway through auto-phosphorylation. INSRα is expressed as isoforms A and B due to alternative splicing (exon 11 is spliced for isoform B). (**C**) Human INSR is colocalized with claudin-5 and collagen IV in brain microvessels and hippocampal section, whereas no colocalization was observed with NeuN-labelled neurons in microvessel-depleted fractions (magnification ×20, scale bar = 20 µm). (**D**–**M**) Dot plots of the concentrations of INSR forms in microvessels comparing participants based on neuropathological diagnosis following the ABC criteria (**D**–**H**) or clinical diagnosis (**I**–**M**). Unpaired *t*-test ($$P < 0.05$) or one-way ANOVA followed by Tukey's *post hoc* test (**$P < 0.01$). (**N**) Correlation between the levels of vascular INSRα-B and the global cognitive score. Linear regression analyses were controlled for educational level, age at death, sex and apoE genotype. *F* ratio and *P*-value are shown. (**O** and **P**) Dot plots of the concentrations of pro-INSR and INSRα-B in microvessels comparing APOE4 carriers based on the ABC neuropathological diagnosis. Welch-ANOVA followed by Dunnett's *post hoc* test (¤$P < 0.05$). (**Q**) Representative western blots of consecutive bands are shown. Data were log transformed for statistical analysis and are represented as scatter plots with a logarithmic scale. Horizontal bars indicate mean ± SEM. ABC = Dx Neuropathological Diagnosis; A-AD = Alzheimer's disease; ColIV = Collagen-IV; C = Control; Clinical Dx = Clinical Diagnosis; CypB = Cyclophilin B; EC = Extracellular; IC = Intracellular; O.D. = optical density; P = Microvessel-depleted parenchymal fraction; T = Total homogenate; Va = Vascular fraction enriched in microvessels.

ELISA for human Aβ and APP-βCTF

Concentrations of β-secretase-derived βAPP fragment (APP-βCTF or C99) in detergent-soluble extracts of brain microvessels (parietal cortex) were determined using Human APP-βCTF ELISA Assay kit (IBL) according to the manufacturer's instructions.

Statistical analysis

Statistical analyses were performed using GraphPad Prism 9.0 and JMP 15 software packages. The threshold for statistical significance was set to $P < 0.05$. Homogeneity of variance and normality were determined for all data sets using D'Agostino and Pearson's or Shapiro–Wilk normality tests. When normality was verified, unpaired Student's t-tests were used to identify significant differences between two groups. Otherwise, the Welch correction or a Mann–Whitney test was performed. When more than two groups were compared, parametric one-way ANOVA followed by Tukey's multiple comparison tests were performed unless variances were different, in which case Welch-ANOVA followed by Dunnett's multiple comparison tests were used. When both normality and variance equality were not confirmed, a non-parametric Kruskall–Wallis test followed by Dunn's multiple comparison was performed. Relative optical density values obtained were log transformed when needed to reduce variances and provide more normally distributed data when appropriate. For insulin stimulation experiments, data were presented as a percentage of the control group to facilitate the comparison of INSR activation between groups. For ISCP experiments, a ROUT test (Q = 1%) available on GraphPad Prism was performed to determine outliers. Multivariate analyses were used to assess the association between continuous variables. Significance of correlations with ante-mortem clinical scores were adjusted for the following covariates: education level, sex, age at death and Apolipoprotein E (APOE) genotype.

Study approval

All procedures performed with volunteers included in this study were in accordance with the ethical standards of the institutional ethics committees and with the 1964 Helsinki Declaration. Written informed consent was obtained from all individual participants included in this study. All procedures relating to mouse care and experimental treatments were approved by the Laval University animal research committee (CPAUL) in accordance with the standards of the Canadian Council on Animal Care.

Data availability

The data that support findings of this study are available from the corresponding author on reasonable request. Data from the ROS can be requested at https://www.radc.rush.edu. Database of gene expression in adult brain and perivascular cells are available at http://betsholtzlab.org/VascularSingleCells/database.html (Betsholtz laboratory), and for human (control and AD) at https://twc-stanford.shinyapps.io/human_bbb/ (Tony Wyss-Coray laboratory).

Results

INSRs are enriched in human brain microvessels: levels of the isoform INSRα-B are reduced in Alzheimer's disease

To determine the post-mortem localization of the INSR in the human brain, we first extracted microvessels from parietal cortex samples collected from ROS participants. We opted for a soft procedure using sequential centrifugation and filtration steps, adapted for frozen samples, as previously described.[54,55] We observed that INSR were present in higher concentrations in vascular fractions (Va) containing brain microvessels, compared to microvessel-depleted parenchymal fractions (P) and whole brain homogenates (T) (Fig. 1A). The validity of the method was confirmed by the coinciding enrichment in endothelial markers claudin-5, ATP binding cassette protein B1 (ABCB1) (P-gp) and platelet endothelial cell adhesion molecule (CD31) in the same vascular fractions, whereas neuronal nuclei (NeuN) staining was more prominent in microvessel-depleted fractions (Fig. 1A), as shown in our previous work.[54,55]

INSR is a heterotetrametric receptor combining two dimers composed of both α (extracellular) and β (intracellular) chains, recognizable by different antibodies (Fig. 1B and Supplementary Table 2) but all coded from the same *INSR* gene. INSRα incorporates the binding site for circulating insulin and exists in two isoforms depending on the absence or presence of exon 11, depicted as A and B, respectively. The full-size precursor of the INSR, pro-INSR and both INSRα and INSRβ isomers were all enriched in vascular fractions (Fig. 1A).

The localization of INSRα on microvessels was confirmed by confocal immunofluorescence where the signal of human INSRα antibody overlapped with claudin-5, a tight-junction protein of brain endothelial cells, but was almost absent in microvessel-depleted fractions containing NeuN-positive cells (Fig. 1C and Supplementary Fig. 3). In addition, immunosignals for INSRβ and collagen IV, a basal membrane protein, colocalized in human microvessels from microvascular-enriched fractions and brain sections (Fig. 1C).

Western blot analyses revealed that INSRα-B levels were lower in vascular fractions from participants with a neuropathological (–48%) or clinical (–40% and –59% compared to NCI and MCI, respectively) diagnosis of Alzheimer's disease, but not significant versus Controls (Fig. 1G and L). Whereas levels of pro-INSR, INSRβ or INSRα-A did not differ (Fig. 1D–F and I–K). A lower INSRα-B was also found in association with Thal, Braak and CERAD ratings (Supplementary Fig. 4). In the parenchymal fractions, where the INSRα B isoform was absent, levels of the INSRα A isoform were not different between groups (Supplementary Fig. 2). Interestingly, participants with a neuropathological or clinical diagnosis of Alzheimer's disease had a higher vascular INSRα-A/B ratio (Fig. 1H and M), a molecular index of insulin resistance in the liver and adipose tissue.[12,82–85] In addition, ante-mortem global cognition was positively correlated with the cerebrovascular content in INSRα-B (Fig. 1N), but not to other INSR isoforms (Supplementary Fig. 5). No significant association between INSR levels and age of death (Supplementary Table 1) was observed. Finally, participants with Alzheimer's disease carrying one apoE4 allele had lower concentrations of pro-INSR (–83% and –83%) and INSRα-B (–40% and –56%) compared to Alzheimer's disease non-carriers and control participants, respectively (Fig. 1O and P). Immunoblots are shown in Fig. 1Q and in Supplementary Fig. 2.

Levels of vascular INSR correlate with Aβ pathology or BBB proteins involved in Aβ production and clearance

We next investigated the association between vascular INSR and several markers of Aβ pathology previously assessed in whole homogenates and/or in microvascular extracts from the parietal

cortex from the same series of ROS participants (Fig. 2A).[55,67,68] Significant inverse correlations were found between vascular levels of INSRα-B, neuritic plaques, as well as vascular β-secretase (BACE1, β-secretase-derived βAPP fragment), an enzyme implicated in APP cleavage and Aβ formation (Fig. 2B and C). By contrast, INSRα-B levels in vascular extracts were positively correlated with vascular neprilysin and insulin-degrading enzyme (IDE), two enzymes involved in Aβ degradation (Fig. 2A and D). In addition, strong associations were detected between vascular INSRα-B, ABCB1 (P-gp) and low-density lipoprotein receptor-related protein 1 (LRP1), implicated in Aβ efflux,[86,87] suggesting that more INSRα-B at the BBB is associated with a higher clearance of Aβ from brain to blood (Fig. 2A and E). However, soluble and insoluble levels of $Aβ_{40}$ or $Aβ_{42}$ in parietal cortex proteins homogenates did not show any association with vascular INSRα-B. A positive association between INSRβ and total soluble tau [$F(1,50) = 7.92$; $P = 0.0079$] and an inverse association with neurofibrillary tangles [$F(1,50) = -7.10$; $P = 0.0141$] were observed, but not with total insoluble tau or other forms of INSR (Fig. 2A). Of note, total soluble tau does not differentiate Alzheimer's disease versus control in this cohort, whereas insoluble total tau and neurofibrillary tangles are higher in Alzheimer's disease (Supplementary Table 1).[67,68] Finally, we noted that INSRα-B and most of the other INSR isoforms were positively associated with caveolin-1 and endothelial nitric oxide synthase (eNOS), two proteins involved in receptor recycling and endothelial generation of nitric oxide, respectively (Fig. 2A, F and G).

INSR is altered in 3xTg-AD mouse microvessels

To assess the localization of INSR in the mouse brain, we performed the same extraction procedures used with human samples. We observed a vascular enrichment for all isoforms, but stronger for pro-INSR and INSRα-B, compared to total homogenates or microvessel-depleted parenchymal fractions (Fig. 3A), corroborating human data. The INSRα-A/B ratio in brain microvessels was lower in mice compared to humans (Figs 1A and 3A). The concomitant enrichment of endothelial markers claudin-5, CD31 and ABCB1 (P-gp) in vascular fractions validated the method.

To determine whether changes in INSR are a consequence of classical Alzheimer's disease neuropathology, we applied the same methodology to brain samples from 3xTg-AD mice at different ages (6, 12 and 18 months). Multivariate analyses showed that the 3xTg-AD genotype was associated with lower INSRα-A or pro-INSR levels, although differences at each age remained non-significant (Fig. 3B, D and G). Similar to the findings in human microvessel extracts, no difference between groups was observed for INSRβ (Fig. 3C and G). Interestingly, INSRα-B levels in microvessel-enriched fractions were lower in 3xTg-AD mice at 18 months of age compared to non-Tg mice (-51.1%), in accordance with human data (Fig. 3E and G). A significant linear trend from 6 to 18 months ($r^2 = -0.1828$, $P = 0.0116$) and a genotype–age interaction were detected, consistent with an age-induced decrease of INSRα-B only in 3xTg-AD animals (Fig. 3E and G). By contrast, we also found a significant genotype–age interaction for vascular BACE1, associated with a linear upward trend with age in 3xTg-AD mice ($r^2 = 0.2130$, $P = 0.0076$) (Fig. 3F and G). These results unveil a pattern of changes of INSR, particularly INSRα-B, induced by age and Aβ/tau pathologies, in agreement with human data.

The insulin-induced activation of INSR at the BBB is blunted in 3xTg-AD mice

Our results so far indicate that cerebral INSR are concentrated in microvessels, but with levels decreasing along with Alzheimer's disease pathology. Previous published data indicate that Alzheimer's disease is associated with reduced activation of INSR and its downstream intracellular signalling.[4,20,21] However, it remains to be shown where blood-borne insulin activates INSRs in the brain, and whether this activation is disturbed by Alzheimer's disease pathology. Like other members of the tyrosine kinase family of receptors, the binding of an agonist triggers autophosphorylation of the INSR. However, its implication as a transporter to ferry circulating insulin into the brain parenchyma has been recently disputed.[8] We thus directly assessed the transport of insulin through the BBB using intracarotid ISCP, with or without an INSR-specific competitive antagonist S961 (Fig. 4A). Perfused ^{125}I-insulin was set at 0.1 nM, close to the physiological concentration of circulating insulin in the mouse.[88,89] We found that the brain uptake coefficient of ^{125}I-insulin was very low (0.028 ± 0.007 µl/g·s) compared to a highly diffusible compound such as diazepam (45.6 ± 2.6 µl/g·s). In addition, S961 (20 nM) did not block ^{125}I-insulin transport. We also confirmed that neither insulin nor S961 had an impact on BBB permeability using ^{3}H-sucrose (Fig. 4A and B). Finally, 3xTg-AD transgenes had no significant impact on ^{125}I-insulin transport or BBB integrity in 13.5-month-old mice (Fig. 4C). These data indicate that INSR at the BBB does not act as the main transporter for insulin, in accordance with published *in vitro* and *in vivo* data.[50,51,90]

Next, we used ISCP to infuse insulin in the carotid, to assess the activation of cerebral INSR *in vivo* and compare microvessel-enriched versus parenchymal fractions. We first showed that, in 6-month-old C57Bl6 mice, intracarotid administration of insulin (0.4 mg/kg or 350 nM) triggers phosphorylation of tyrosine residues (Y1150/1151) on INSRβ within 120 seconds compared to the same physiological buffer without insulin (Fig. 4D). Faster acting Aspart insulin NovoRapid® and regular insulin Novolin®ge Toronto (350 nM) were compared and both led to the phosphorylation of INSR (Fig. 4D and Supplementary Fig. 6). Strikingly, this activation of INSRβ was only observed in microvascular extracts, while no trace was detected in the parenchymal fraction despite low but detectable levels of INSRs (Fig. 4D). This result indicates that INSR at the BBB is activated by circulating insulin and is consistent with a brain response to circulating insulin occurring predominantly at the BBB level, not in parenchymal cells.

To assess whether the activation of INSR is altered by Aβ and tau neuropathologies, we performed the same intracarotid insulin injection experiments in 3xTg-AD mice followed by microvessel isolation and immunoblotting. While insulin-induced phosphorylation of INSRβ in microvessels of 16-month-old non-Tg mice, such activation was greatly attenuated in 3xTg-AD mice of the same age (Fig. 4E and M), with both types of insulin used (hexameric Novolin®ge Toronto or monomeric Aspart insulin NovoRapid®). In contrast, levels of INSRβ or pro-INSR were similar between groups (Fig. 4F, G and M). Replicating the data shown in Fig. 3E in 18-month-old 3xTg-AD mice, INSRα-B concentrations in vascular extracts were lower in this group of 15-month-old 3xTg-AD mice (Fig. 4H and M). The vascular INSRα-A/B ratio was higher in 3xTg-AD mice, further supporting insulin resistance at the level of the BBB (Fig. 4I and M).

We also assessed the effect of intracarotid insulin on other vascular proteins in non-Tg and 3xTg-AD mice and no difference was found in the levels of BACE1, neprilysin, IDE and other Aβ transporters (P-gp/ABCB1, LRP1 or receptor for advanced glycation

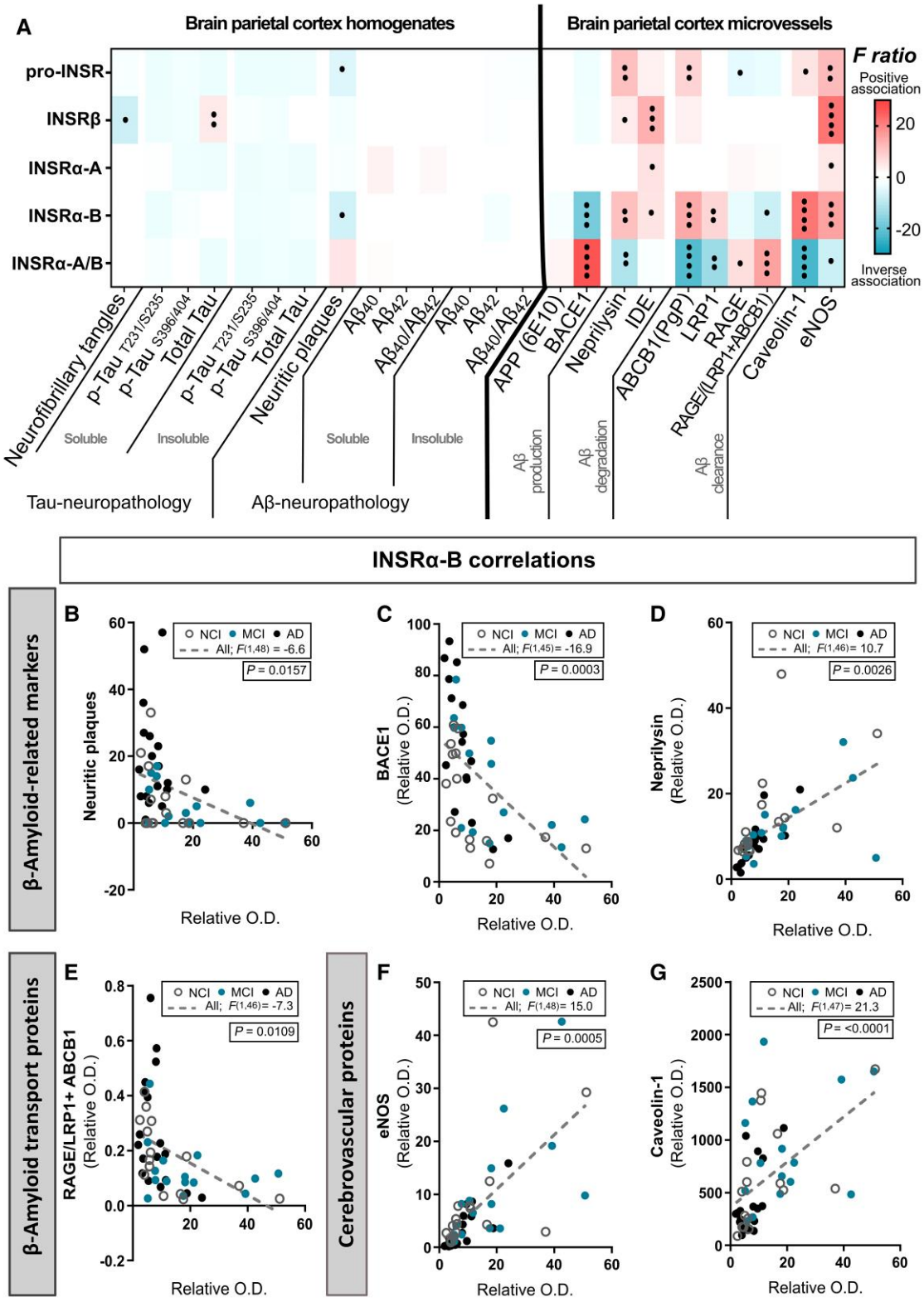

Figure 2 Cerebrovascular levels of INSRα-B correlate with neuritic plaques and Aβ-related proteins located on the BBB. (**A**–**G**) Correlations between cerebrovascular INSRs and neurofibrillary tangle counts, phosphorylated-tau T231/S235 (AT180), S396/404 (AD2, confirmed with PHF1) (Tau neuropathology), cortex neuritic plaque counts and Aβ concentrations (Aβ-neuropathology) in brain homogenates. Correlations were also established with other proteins assessed in microvessel-enriched fractions. Soluble and insoluble proteins are found in TBS-soluble and formic acid-soluble fractions, respectively. Linear regressions analyses were controlled for educational level, age at death, sex and ApoE genotype, and were performed to generate *F*-ratios and *P*-values in the heatmap (•$P < 0.05$; ••$P < 0.01$; •••$P < 0.001$; ••••$P < 0.0001$). Red and blue highlighted cells, respectively, indicate significant positive and negative correlations (**A**). Graphical representation of noteworthy correlations between INSRα-B and Aβ-related markers (**B**–**D**) and transporters (**E**), as well as microvessel markers (**F** and **G**). APP = amyloid precursor protein; O.D. = optical density; RAGE = receptor for advanced glycation end products.

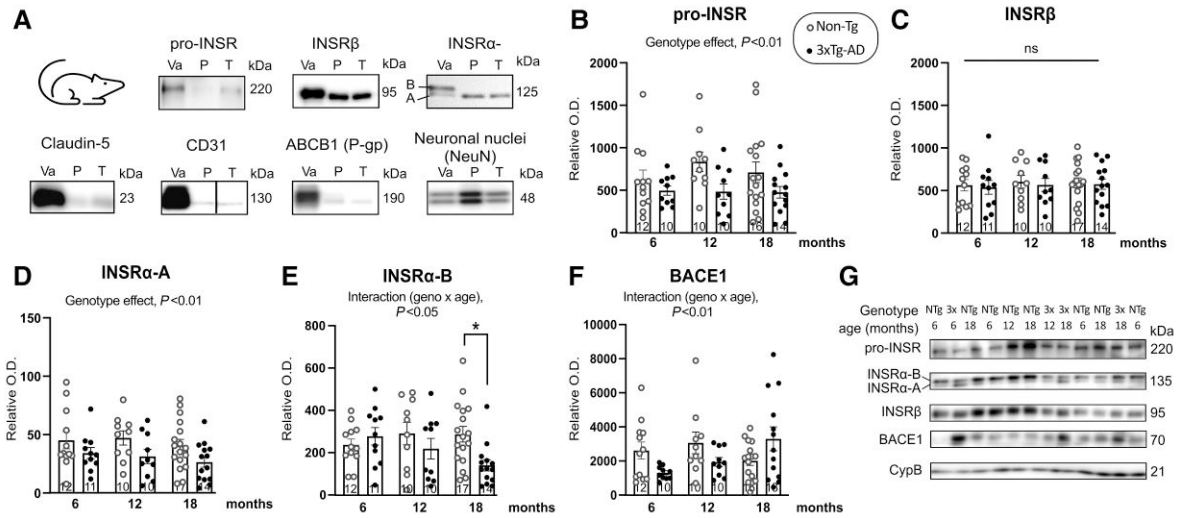

Figure 3 Lower vascular INSR in old 3xTg-AD mice. (**A**) Representative western blots showing enriched content in pro-INSR, INSRα and INSRβ in vascular fractions compared to parenchymal fractions (rich in neuronal marker NeuN) and total homogenates from the mouse brain, along with known endothelial markers claudin-5, CD31 and ABCB1(P-gp). (**B–F**) Vascular levels of pro-INSR, INSRβ, INSRα-A, INSRα-B and BACE1 in 3xTg-AD and Non-Tg mice at 6, 12 and 18 months of age (42 males and 34 females). Two-way ANOVA followed by Tukey's *post hoc* test (*$P < 0.05$; ns = non-significant), and linear trend model. Data are presented as mean ± SEM. (**G**) Representative western blots of consecutive bands are shown. 3xTg-AD = tri-transgenic mice; CypB = Cyclophilin B; EC = Extracellular; IC = Intracellular; NTg-Non-Tg = non-Tg mice; O.D. = optical density; P = Microvessel-depleted parenchymal fraction; T = Total homogenate; Va = Vascular fraction enriched in microvessels.

endproducts) (Fig. 4J and M and Supplementary Fig. 6). This is consistent with the 3xTg-AD mouse being a model of Aβ overproduction, rather than a model of reduced Aβ clearance. However, a lower concentration of caveolin-1 was observed in 3xTg-AD compared to non-Tg mice (Fig. 4K–M).

Results of these experiments show that Alzheimer's disease-like neuropathology impairs the activation of vascular INSRs in the 3xTg-AD mouse model. This collection of data indicates that circulating insulin primarily interacts with INSRs exposed on the luminal side of the BBB in both human and mice and that the INSR-mediated response is blunted in Alzheimer's disease.

The reduction of INSR is associated with BACE1 activity in the BBB

The strong inverse correlation between BACE1 and INSR in the neurovascular compartment led us to explore whether a decrease in INSR levels could be a consequence of BACE1 protease activity. The capacity of BACE1 to cleave INSR has been demonstrated in the muscle and liver, therein contributing to insulin resistance.[91] Higher BACE1 cleavage activity of the INSR β-chain has been recently associated with cognitive impairment and type-2 diabetes in a clinical cohort study.[92] BACE1 levels in the cerebrovasculature are higher in Alzheimer's disease and associated with cognitive impairment.[55]

To further assess BACE1 activity in microvessels, we measured the concentration of APPβ-CTF, a marker of BACE1 cleaving activity. Microvascular levels of APPβ-CTF were significantly higher in Alzheimer's disease compared to controls on the basis of the ABC neuropathological diagnosis (Fig. 5A), whereas a similar upwards trend was noted in Alzheimer's disease compared to MCI on the basis of the clinical diagnosis ($P = 0.053$) (Fig. 5B). We first observed a strong positive association between vascular APPβ-CTF and INSRα-A/B ratio [$F(1,40) = 12.6$; $P = 0.002$], and a significant inverse correlation with INSRα-B [$F(1,40) = -10.9$; $P = 0.003$] (Fig. 5C and D). In contrast, vascular APPβ-CTF showed a significant positive correlation with BACE1 [$F(1,42) = 45.7$; $P < 0.0001$] (Fig. 5E). Immunofluorescence experiments confirmed the localization of both BACE1 and $Aβ_{42}$ on capillaries (Fig. 5F and G). These combined data highlight the importance of BACE1 in Alzheimer's disease for both cerebrovascular Aβ pathology and insulin resistance, and suggest a role for BACE1 in cleaving vascular INSR (Fig. 5F–H).

Discussion

The present study provides evidence that INSR is enriched at BBB and could underlie the brain insulin resistance observed in Alzheimer's disease. We specifically show that: (i) vascular INSR defects are linked to Alzheimer's disease pathology and symptoms in humans and that the activation of INSR is reduced by Alzheimer's disease neuropathology in a mouse model; and (ii) INSR located on the BBB is involved in the rapid response to circulating insulin, where it acts as a tyrosine kinase receptor not a transporter. Our data suggest that pancreas-produced insulin interacts primarily with the INSR on the luminal side of the brain vasculature and that its response becomes defective in Alzheimer's disease, possibly following cleavage by BACE1. This highlights a previously unrecognized role of INSR in the cerebral vasculature as a systemically accessible drug target in Alzheimer's disease.

INSR localization in brain microvessels

So far, the exact cellular localization of INSR in the brain has remained uncertain due to conflicting evidence. Autoradiography studies in rat brain sections reported prominent binding levels of ^{125}I-insulin in the hippocampal formation,[36] choroid plexus[38] and hypothalamus,[93] as well as in the olfactory bulb, cerebral cortex and cerebellum.[37] A similar distribution pattern of INSRα was found using *in situ* hybridization in rat brain.[39] Western blot analyses

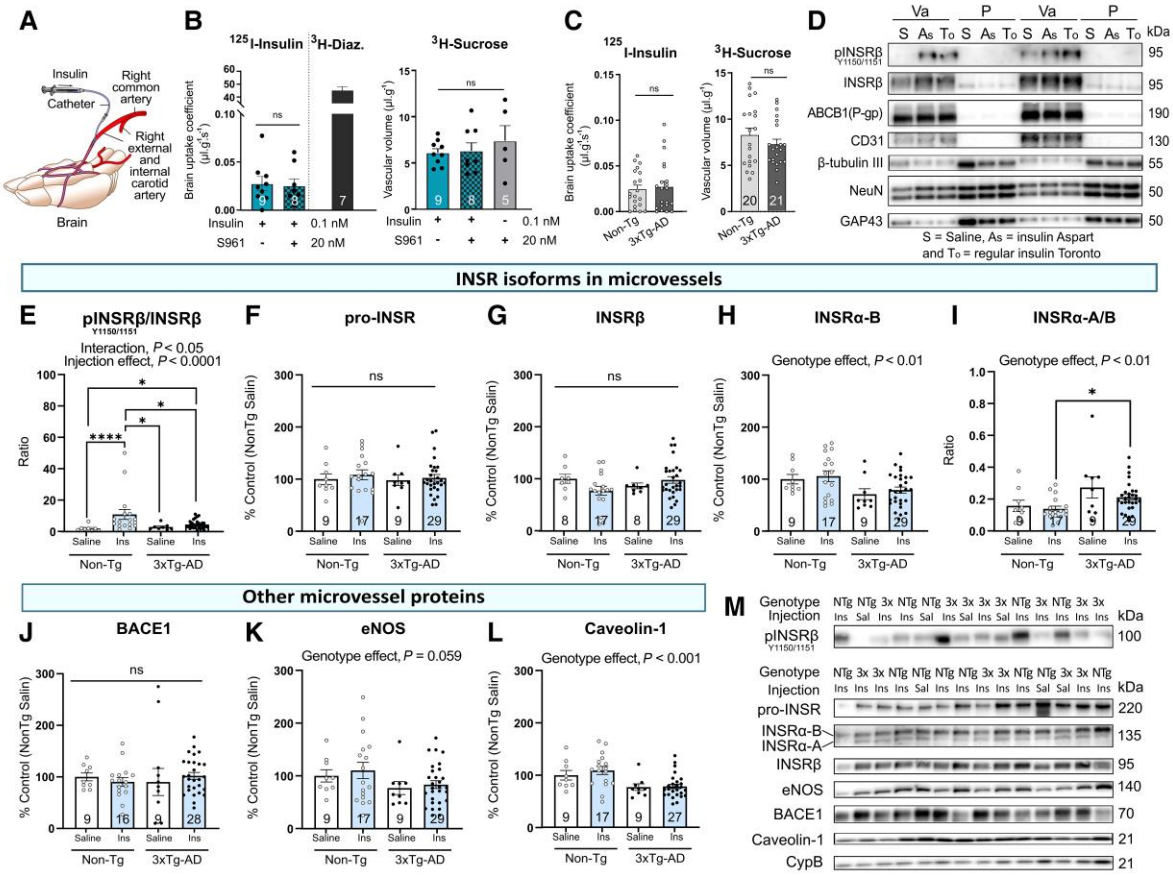

Figure 4 The activation of INSR after intracarotid injection of insulin is restricted to brain microvessels and is blunted in 3xTg-AD mice. (**A**) Illustration of the ISCP technique. (**B**) Brain uptake coefficient of ^{125}I-insulin (0.01 nM) perfused alone or with S961 (20 nM), a selective INSR antagonist competing with insulin, in Balb/c mice aged 15 weeks. ^{3}H-Diazepam (0.3 µCi/µl) was perfused in age-matched C57Bl6 mice to emphasize the difference between a highly diffusible drug and insulin (*left*). No significant change in cerebrovascular volume due to the treatment was observed by coperfusing the vascular marker ^{3}H-sucrose (0.3 µCi/ml) (*right*). Unpaired *t*-test or parametric one-way analysis of variance (ns, non-significant). Data are presented as mean ± SEM. (**C**) Brain uptake coefficient of ^{125}I-insulin (0.01 nM) comparing non-Tg and 3xTg-AD mice aged 13.5 months (*left*). No significant change in cerebrovascular volume due to the treatment was observed by coperfusing the vascular marker ^{3}H-sucrose (0.3 µCi/ml) (*right*). Unpaired *t*-test (ns, non-significant). Data are presented as mean ± SEM. (**D**) Representative western blots showing phosphorylated INSRβ in vascular fractions following perfusion of insulin (Aspart or Toronto) by ISCP in 6-month-old C57Bl6 mice, compared to parenchymal fractions. Endothelial markers CD31 and ABCB1 (P-gp) as well as the neuronal markers β-tubulin III, NeuN and GAP43 and were immunoblotted on the same membranes. (**E–L**) Dot plots of the concentrations of INSR isoforms in microvessels comparing mice based on genotype and insulin perfusion (**E–I**), and cerebrovascular proteins BACE1, eNOS and caveolin-1 (**J–L**). One-way or two-way analysis of variance followed by Tukey's *post hoc* test (*$P < 0.05$; ****$P < 0.0001$). Data were log transformed for statistical analysis. Outliers were removed from statistical analyses as described in the 'Methods section'. Horizontal bars indicate mean ± SEM. (**M**) Representative western blots of consecutive bands are shown, from the same samples, but from a different randomization. 3xTg-AD = tri-transgenic mice; As = insulin Aspart (NovoRapid®); CypB = Cyclophilin B; Diaz = Diazepam; Ins = insulin perfusion; GAP43 = Growth Associated Protein 43; NTg-Non-Tg = non-Tg mice; P = Microvessel-depleted parenchymal fraction; S961 = INSR antagonist; S-Sal = saline perfusion; To = regular insulin Toronto (Novolin® ge); Va = Vascular fraction enriched in microvessels.

detected INSRα in the human cerebral cortex and hippocampus but not in the white matter.[35] These studies, however, did not provide insights on the cellular location of the receptor. Initial studies performed by a single group using IHC in paraformaldehyde-fixed brain sections reported a localization of INSRβ in different areas of the rat forebrain (olfactory bulb, hypothalamus and hippocampus), largely exhibiting localization in cells resembling neurons.[33,34] However, more recent studies with RNA sequencing in mouse and human brain cells showed that INSR is largely expressed in endothelial and glial cells.[40–42] An older study with autoradiograms of ^{125}I-insulin hinted toward a 130-kDa doublet corresponding to isoforms -B and -A of INSRα located in cerebral microvessels.[10] These discrepancies may be explained by a recurring challenge in the difficulty of finding appropriate antibodies for the INSR, and its isoforms, particularly when using human samples.

The present set of data indicates that most INSR isoforms in the human and mouse brain are predominantly localized in microvessels, and this was particularly the case for the isoform INSRα-B, which was virtually absent from the brain parenchyma. Beside this preferential localization of INSR in microvessels, which has been underestimated in previous years, a significant fraction of INSR is also present in other cells within the parenchyma, where they can interact with low levels of insulin in the brain interstitial fluid. Indeed, cultured astrocytes and neurons respond to insulin, and cell-specific knockouts demonstrate that removing INSR from these cells affects insulin signalling *in vivo*.[94–99] Thus, our results do not rule out a key role of INSR located on neurons or astrocytes. Nonetheless, they indicate that BBB INSR is probably the primary cerebral target that responds to insulin circulating in the blood after secretion by the pancreas.

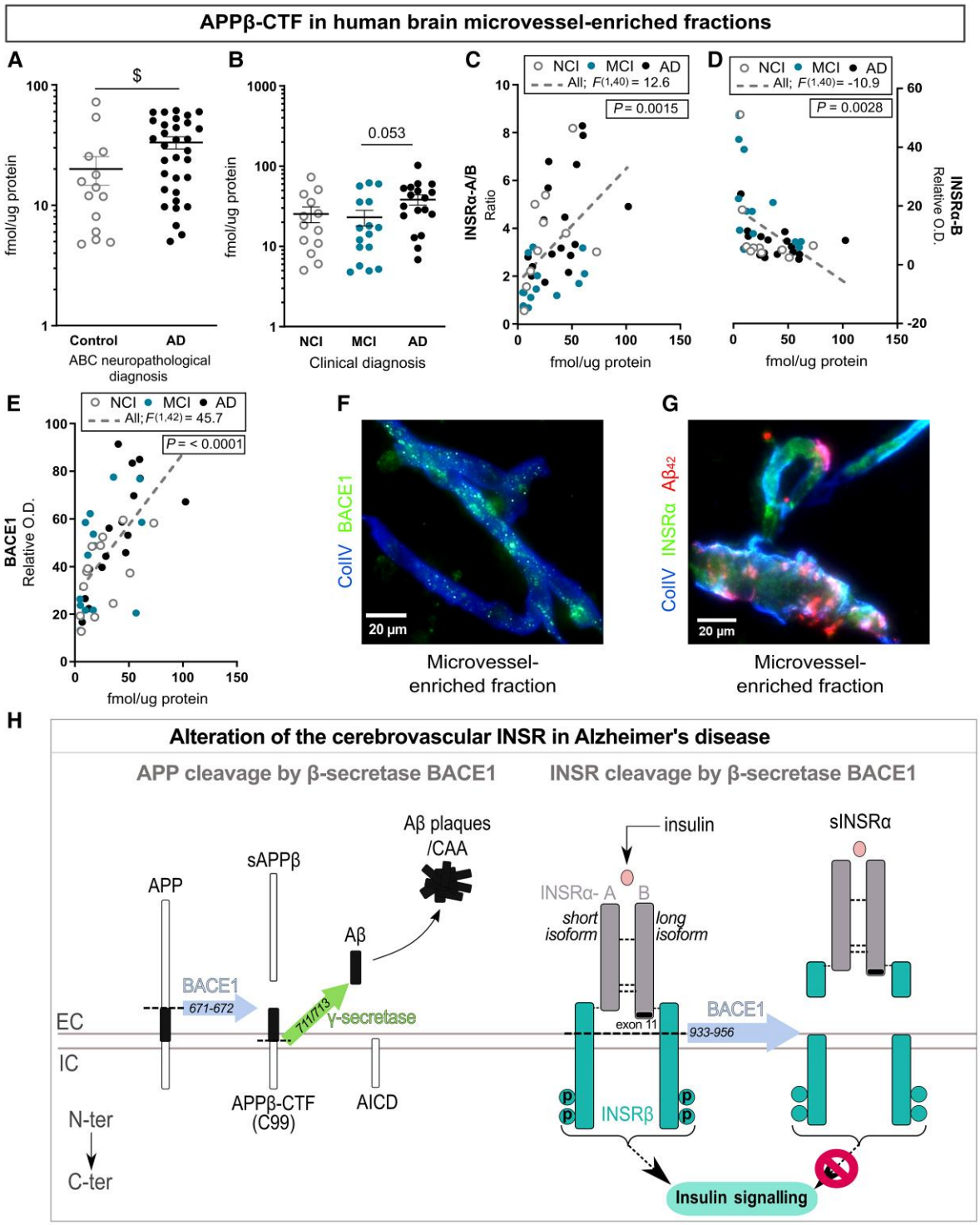

Figure 5 BACE1 cleavage product APPβ-CTF is negatively associated with human neurovascular levels of INSRα-B. (**A** and **B**) Dot plots of the concentrations of APPβ-CTF in microvessels comparing participants based on neuropathological diagnosis following the ABC criteria (**A**) or clinical diagnosis (**B**). Unpaired *t*-test ($*P* < 0.05$) or parametric one-way analysis of variance followed by Tukey's *post hoc* test. Data were log transformed for statistical analysis and are represented as scatter plots with a logarithmic scale. Horizontal bars indicate mean ± SEM. (**C–E**) Correlations between the levels of vascular APPβ-CTF, INSRα-A/B ratio, INSRα-B and BACE1, in human brain vascular fractions. Linear regression analyses were controlled for educational level, age at death, sex and ApoE genotype. *F*-ratio and *P*-values are shown. (**F**) Representative immunofluorescence labelling of human INSRα showing the colocalization with $Aβ_{42}$ and collagen IV in brain microvessels of an Alzheimer's disease patient with stage 4 cerebral amyloid angiopathy (CAA) pathology (magnification ×40, scale bar = 20 µm). (**G**) Representative immunofluorescence labelling of BACE1 showing its colocalization with collagen IV in brain microvessels of an Alzheimer's disease patient (magnification ×20, scale bar = 20 µm). (**H**) Illustration of the role of β-secretase in cleaving APP and, hypothetically, INSR in the brain vasculature of Alzheimer's disease patients. ABC Dx = neuropathological diagnosis; AD = Alzheimer's disease; APP = amyloid precursor protein; APPβ-CTF = β-secretase-derived βAPP C-terminal fragment; AICD = amyloid precursor protein intracellular domain; BACE1 = β-site APP cleaving enzyme; CAA = cerebral amyloid angiopathy; Clinical Dx = clinical diagnosis; ColIV = collagen IV; EC = extracellular; IC = intracellular; O.D. = optical density; sAPPβ = β-secretase-derived βAPP soluble fragment.

Microvascular INSR at the BBB as the site of brain insulin resistance in Alzheimer's disease

The lower levels of vascular INSRα-B in subjects with either a neuropathological or clinical diagnosis of Alzheimer's disease, which were inversely associated with cognitive scores, can be interpreted as a sign of brain insulin resistance in Alzheimer's disease. Although the INSRα-B isoform was reduced, pro-INSR, INSRβ and INSRα-A did not differ significantly between groups. No association between cerebrovascular INSR and age was found in the ROS cohort, contrasting with previous studies that reported dysregulation of circulating insulin and reduced transport, binding and signalling in the brain with ageing.[44,100–106] We found corroborating data in old 3xTg-AD mice, where INSRα-B was decreased at 18 months of age compared to non-Tg controls. This shift towards a higher INSRα-A/B isoform ratio at the BBB in Alzheimer's disease may have mechanistic implications. INSR isoforms have been the subject of more scrutiny in peripheral organs (muscle, adipose tissue and liver), in cancers and in metabolic diseases, such as obesity and diabetes.[83–85,107–109] Whereas the cellular implication of a change in INSRα-A/B ratios remains unclear, the short INSRα-A is preferentially expressed in foetal tissues containing proliferating cells (growth signal) and INSRα-B is predominant in adult tissue in differentiated cells (metabolic signal).[12] INSR formed of INSRα-A or -B isoforms would show a dissimilar affinity for insulin or tyrosine kinase activity according to some but not all studies.[12–14,110–112] Higher INSRα-A/B ratios are observed in adipocytes from obese patients and in the liver from patients with type-2 diabetes, both returning to normal after weight loss and diabetes remission.[83,84] Therefore, a higher INSRα-A/B ratio in insulin sensitive organs has been proposed as a molecular index of insulin resistance.[12] In sum, the observed higher vascular INSRα-A/B ratio can be interpreted as a sign of insulin resistance in the cerebrovasculature, possibly hindering the capacity of the INSR to trigger intracellular events/signalling in Alzheimer's disease.

Circulating insulin activates INSR in microvessels but not in the parenchyma: this activation is blunted in animal models of Alzheimer's disease

One of the main observations reported here is that the phosphorylation of INSRβ after direct intracarotid infusion of insulin was detected at the BBB level and not in the parenchyma. Despite the presence of INSRs and neurons in the parenchymal fractions, no evidence of increased phosphorylation of INSRβ was detected even at a very high dose. This suggests that the physiological short-lived peak of insulin in the blood, typically observed after a meal, exerts most of its action on INSR located on the BBB and less in neurons. Whereas most cells in microvessel extracts are BCEC[54,55] containing INSR mRNA transcripts,[40–42] it is important to note that pericytes and astrocyte feet are also present in smaller amounts. It is notable that this insulin-induced INSRβ phosphorylation, observed in all control mice, was greatly attenuated in brain microvessels from 3xTg-AD mice, indicating that Alzheimer's disease neuropathology impairs INSR signalling. This defect in INSR signalling was observed even with the high concentration of insulin used. Previous studies using post-mortem *ex vivo* stimulation of whole brain human slices with insulin have reported lower phosphorylation of INSRβ (Y1150/1151 and Y960) in the cerebellar cortex and the hippocampal formation in Alzheimer's disease patients.[21] However, similar studies performed in the middle frontal gyrus cortex did not find associations between p-INSRβ and diabetes, Aβ burden, tau tangle density or cognitive scores, although pS^{473} AKT1 was associated with less angiopathy.[20,113] Although post-mortem human data cannot be used to infer any causal relationship, which may be bidirectional, changes in INSR levels and signalling observed in old 3xTg-AD mice are likely to be a consequence of Alzheimer's disease-like pathology and/or transgenes, and perhaps related to the other metabolic defects reported in this model.[22,73,76,78,114] The present results suggest that INSRs located on microvessels contribute to the previously reported evidence of central insulin resistance in Alzheimer's disease.

Of note, INSR isoforms can form hybrids with IGF-1 receptors (IGF-1R),[36,37,115,116] and lower IGF-1R levels and impaired signalling have been associated with Aβ and tau neuropathology in the brain of Alzheimer's disease patients.[117–121] Along with INSR, lower IGF-1R phosphorylation was observed following *ex vivo* stimulation with insulin in hippocampal sections from Alzheimer's individuals.[21] Interestingly, insulin displays a greater affinity for INSRα-B homodimers compared to INSRα-A homodimers and hybrid receptors.[110,122] Further studies are thus warranted to determine the contribution of IGF-1R alone or within INSR/IGF-1R complexes, in the response of the brain to insulin, particularly in Alzheimer's disease.

One must also keep in mind that the ISCP paradigm used here detects the acute effect of insulin that reaches the BBB interface. Longer exposure times to insulin may be necessary to transmit an effect to neurons deeper in the brain parenchyma. However, a report using hyperglycaemia clamp and microdialysis showed that a longer peripheral exposure to insulin did not result in increased insulin levels in brain interstitial fluid, nor in higher hippocampal Akt phosphorylation.[123]

The loss of INSR is associated with a pattern of protein changes implying lower clearance and higher production of Aβ

Our report highlights the possible association between vascular INSR levels and an altered equilibrium between production and clearance of Aβ at the level of the BBB. On the one hand, INSRα-B was found to be positively associated with ABCB1 (P-gp) and LRP1, two endothelial proteins involved in Aβ efflux from the parenchyma through the BBB to the blood.[55,86,87] Similar relationships were found with neprilysin and IDE, two key enzymes involved in Aβ degradation. Neprilysin levels were previously found to be reduced in Alzheimer's disease microvessels,[55,124] while Aβ can be a substrate of IDE competing with insulin.[125,126] While cerebrovascular INSRα-B was associated with neuritic plaque counts in the cortex and Aβ clearance proteins in the BBB, no such relationship was detected with $Aβ_{42}$ concentrations. This may suggest that other variables are in play in the regulation of brain Aβ levels, such as alternative clearance pathways.[55,127,128] Published mechanistic data show that Aβ (i) can promote lysosomal degradation of INSR in 3xTg-AD murine and porcine brain capillaries[43]; and (ii) acts as a competitive antagonist of insulin to the INSR, thereby contributing to insulin resistance.[16,129] On the other hand, INSRα-B was negatively correlated with BACE1, a β-secretase initiating the cleavage of amyloid precursor protein (APP) and formation of APPβ-CTF and Aβ[130]: both of which are found in higher concentrations in Alzheimer's disease brain or microvessels.[55,131–133] Using induced pluripotent stem cell (iPSC) neurons carrying APP and/or PSEN1 familial Alzheimer's disease mutations, a recent study reported that BACE1-produced APPβ-CTF alter endosomal and intracellular trafficking, which might contribute to BBB defects.[134] Finally, BBB

INSRα-B was also associated with levels of endothelial nitric oxide synthase (eNOS or NOS3) and caveolin-1, two Alzheimer's disease-relevant vascular proteins involved in insulin uptake, INSR trafficking and signalling.[135,136] Altogether, these observations indicate that the preservation of INSR signalling in the BBB is associated with increased clearance of Aβ, lower BACE1 activity, neurovascular integrity and sustained cognitive performance.

What is the cause of INSR decrease in Alzheimer's disease?

Overall, these series of observations are consistent with the hypothesis that Alzheimer's disease is accompanied by a reduction in binding sites available to circulating insulin at the level of the BBB. Several mechanisms can explain the observed decrease in INSRα-B. First, we found corroborating data in old 3xTg-AD mice, where INSRα-B was decreased at 18 months of age with no changes in INSRβ. This suggests that age and Alzheimer's disease neuropathology are involved. Second, it could be proposed that microvascular cells expressing INSRs are specifically lost in Alzheimer's disease. This hypothesis is, however, unlikely, as we did not find a significant reduction in endothelial cells in this cohort as assessed with claudin-5, CD31 or CypB.[55] A third explanation involving a change at the gene transcription level is also unlikely since the decrease was specific to the isoform INSRα-B, whereas INSRα-A, INSRβ and pro-INSR were mostly unaffected. Fourth, preferential alternative splicing of INSR or isoform-specific conversion could be at play, but underlying mechanisms are not fully understood and little studied in the field of neurology.[12,137,138] Candidate splicing factors and protein convertases are expressed at low level in BCEC and their activity could underlie the specific reduction in INSRα-B observed here.[40,41,139] Overall, we postulate that post-translation modifications are more likely to underlie the observed decrease of the long isoform INSRα-B.

The strength of the correlation between vascular levels of BACE1 and INSRα-B, as well as the vascular INSRα-A/B ratio, was remarkable. A strong association was also established between INSRα-B and the concentration of APPβ-CTF, which is considered as an index of BACE1 activity.[130,134,140] BACE1 is probably the most studied enzyme in Alzheimer's disease, due to its role in the production of Aβ and subsequent accumulation in the brain.[132,133] BACE1 is also expressed in microvascular endothelial cells,[40,41,139,141] in higher concentrations in persons with Alzheimer's disease, correlating with cognitive impairment.[55] However, BACE1 is not only involved in the cleavage of APP, but it also has multiple other substrates, including INSR.[140] Indeed, reports indicate that INSR is the target of proteases, such as calpain 2 and presenilin 1 (γ-secretase), but also BACE1, which has been previously proposed as a mechanism of regulation of INSR signalling.[91,142,143] Notably, studies in the liver show that BACE1 cleaves INSR between amino acids 933–956 of the β-chain, disturbing insulin signalling and generating a soluble fragment (sINSRα, insulin receptor soluble fragment).[91,143] In the liver of db/db mice, higher BACE1 protein and mRNA levels, combined with the generation of sINSRα was observed.[91] Conversely, BACE1$^{-/-}$ mice have significantly less plasma sINSRα and higher liver INSRβ levels.[91] More recent data suggest that BACE1 cleaving activity of INSR may be related to cognitive impairment and type-2 diabetes. The elevated plasma levels of BACE1 were found to correlate with the generation of sINSRα and glycemia in diabetics patients (Type I and II).[92,144] In addition, increased plasma BACE1 activity was proposed as a biomarker for predicting the conversion from MCI to Alzheimer's disease.[145] Keeping these published data in mind, the series of strong correlations between BACE1 levels, BACE activity index (APPβ-CTF) and INSR levels, all measured in cerebral microvessel extracts, suggest a mechanistic scheme in which BACE1-mediated cleavage of INSR contributes to insulin resistance in Alzheimer's disease. A favourable clinical implication is that drugs may not need to fully cross the BBB to alter INSR posttranslational modifications or to mimic the action of pancreas-secreted insulin on the brain.

Acknowledgements

The authors are thankful to Gregory Klein, from the Rush Alzheimer's Disease Research Center, for his assistance with data related to our cohort. The authors are indebted to the nuns, priests and brothers from the Catholic clergy involved in the ROS.

Funding

This work was supported the Canadian Institutes of Health Research (CIHR) to F.C. (grant number PJT 168927). The study was supported in part by P30AG10161, P30AG72975 and R01AG15819 (D.A.B). F.C is a Fonds de recherche du Québec-Santé (FRQ-S) senior research scholar. M.L. was supported by a scholarship from the Fondation CHU de Québec. P.B held scholarships from the Fondation du CHU de Québec, a joint scholarship from the FRQ-S and the Alzheimer Society of Canada (ASC) and a scholarship from the CIHR. V.C. was supported by a scholarship from Fonds d'Enseignement et de la Recherche (FER) from the Faculty of Pharmacy, Laval University.

Competing interests

The authors report no competing interests.

Supplementary material

Supplementary material is available at *Brain* online.

References

1. Lewis GF, Brubaker PL. The discovery of insulin revisited: Lessons for the modern era. *J Clin Invest*. 2021;131(1):e1422399.
2. Polyzos SA, Mantzoros CS. Diabetes mellitus: 100 years since the discovery of insulin. *Metabolism*. 2021;118:154737.
3. Heni M, Kullmann S, Preissl H, Fritsche A, Häring H-U. Impaired insulin action in the human brain: Causes and metabolic consequences. *Nat Rev Endocrinol*. 2015;11:701–11.
4. Arnold SE, Arvanitakis Z, Macauley-Rambach SL, *et al*. Brain insulin resistance in type 2 diabetes and Alzheimer disease: Concepts and conundrums. *Nat Rev Neurol*. 2018;14:168–81.
5. Kellar D, Craft S. Brain insulin resistance in Alzheimer's disease and related disorders: Mechanisms and therapeutic approaches. *Lancet Neurol*. 2020;19:758–66.
6. Moran C, Callisaya ML, Srikanth V, Arvanitakis Z. Diabetes therapies for dementia. *Curr Neurol Neurosci Rep*. 2019;19:58.
7. Banks WA. The source of cerebral insulin. *Eur J Pharmacol*. 2004;490:5–12.
8. Rhea EM, Banks WA. A historical perspective on the interactions of insulin at the blood–brain barrier. *J Neuroendocrinol*. 2021;33:e12929.

9. Frank HJ, Pardridge WM. A direct in vitro demonstration of insulin binding to isolated brain microvessels. *Diabetes*. 1981;30: 757–61.
10. Haskell JF, Meezan E, Pillion DJ. Identification of the insulin receptor of cerebral microvessels. *Am J Physiol Endocrinol Metab*. 1985;248:E115–25.
11. Vicent D, Ilany J, Kondo T, *et al*. The role of endothelial insulin signaling in the regulation of vascular tone and insulin resistance. *J Clin Invest*. 2003;111:1373–80.
12. Belfiore A, Malaguarnera R, Vella V, *et al*. Insulin receptor isoforms in physiology and disease: An updated view. *Endocr Rev*. 2017;38:379–431.
13. Mosthaf L, Grako K, Dull TJ, Coussens L, Ullrich A, McClain DA. Functionally distinct insulin receptors generated by tissue-specific alternative splicing. *Embo J*. 1990;9:2409–13.
14. Yamaguchi Y, Flier JS, Benecke H, Ransil BJ, Moller DE. Ligand-binding properties of the two isoforms of the human insulin receptor. *Endocrinology*. 1993;132:1132–8.
15. Kellerer M, Lammers R, Ermel B, *et al*. Distinct alpha-subunit structures of human insulin receptor A and B variants determine differences in tyrosine kinase activities. *Biochemistry*. 1992;31:4588–96.
16. De Felice FG. Alzheimer's disease and insulin resistance: Translating basic science into clinical applications. *J Clin Invest*. 2013;123:531–9.
17. Baglietto-Vargas D, Shi J, Yaeger DM, Ager R, LaFerla FM. Diabetes and Alzheimer's disease crosstalk. *Neurosci Biobehav Rev*. 2016;64:272–87.
18. de la Monte SM. The full spectrum of Alzheimer's disease is rooted in metabolic derangements that drive type 3 diabetes. *Adv Exp Med Biol*. 2019;1128:45–83.
19. Stanley M, Macauley SL, Caesar EE, *et al*. The effects of peripheral and central high insulin on brain insulin signaling and amyloid-beta in young and old APP/PS1 mice. *J Neurosci*. 2016; 36:11704–15.
20. Arvanitakis Z, Wang HY, Capuano AW, *et al*. Brain insulin signaling, Alzheimer disease pathology, and cognitive function. *Ann Neurol*. 2020;88:513–25.
21. Talbot K, Wang HY, Kazi H, *et al*. Demonstrated brain insulin resistance in Alzheimer's disease patients is associated with IGF-1 resistance, IRS-1 dysregulation, and cognitive decline. *J Clin Invest*. 2012;122:1316–38.
22. Vandal M, White PJ, Tremblay C, *et al*. Insulin reverses the high-fat diet-induced increase in brain Abeta and improves memory in an animal model of Alzheimer disease. *Diabetes*. 2014;63:4291–301.
23. Sanguinetti E, Guzzardi MA, Panetta D, *et al*. Combined effect of fatty diet and cognitive decline on brain metabolism, food intake, body weight, and counteraction by intranasal insulin therapy in 3xTg mice. *Front Cell Neurosci*. 2019;13:188.
24. Craft S, Claxton A, Baker LD, *et al*. Effects of regular and long-acting insulin on cognition and Alzheimer's disease biomarkers: A pilot clinical trial. *J Alzheimers Dis*. 2017;57:1325–34.
25. Kellar D, Lockhart SN, Aisen P, *et al*. Intranasal insulin reduces white matter hyperintensity progression in association with improvements in cognition and CSF biomarker profiles in mild cognitive impairment and Alzheimer's disease. *J Prev Alzheimers Dis*. 2021;8:240–8.
26. Gwizdala KL, Ferguson DP, Kovan J, Novak V, Pontifex MB. Placebo controlled phase II clinical trial: Safety and efficacy of combining intranasal insulin & acute exercise. *Metab Brain Dis*. 2021;36:1289–303.
27. Rosenbloom M, Barclay TR, Kashyap B, *et al*. A phase II, single-center, randomized, double-blind, placebo-controlled study of the safety and therapeutic efficacy of intranasal glulisine in amnestic mild cognitive impairment and probable mild Alzheimer's disease. *Drugs Aging*. 2021;38:407–15.
28. Hölscher C. Protective properties of GLP-1 and associated peptide hormones in neurodegenerative disorders. *Br J Pharmacol*. 2022;179:695–714.
29. Cummings J, Ortiz A, Castellino J, Kinney J. Diabetes: Risk factor and translational therapeutic implications for Alzheimer's disease. *Eur J Neurosci*. Published online 6 Feb 2022. doi:10.1111/ejn.15619
30. Moloney AM, Griffin RJ, Timmons S, O'Connor R, Ravid R, O'Neill C. Defects in IGF-1 receptor, insulin receptor and IRS-1/2 in Alzheimer's disease indicate possible resistance to IGF-1 and insulin signalling. *Neurobiol Aging*. 2010;31:224–43.
31. Lourenco MV, Ferreira ST, De Felice FG. Neuronal stress signaling and eIF2alpha phosphorylation as molecular links between Alzheimer's disease and diabetes. *Prog Neurobiol*. 2015;129:37–57.
32. Frazier HN, Anderson KL, Ghoweri AO, *et al*. Molecular elevation of insulin receptor signaling improves memory recall in aged Fischer 344 rats. *Aging Cell*. 2020;19:e13220.
33. Moss AM, Unger JW, Moxley RT, Livingston JN. Location of phosphotyrosine-containing proteins by immunocytochemistry in the rat forebrain corresponds to the distribution of the insulin receptor. *Proc Natl Acad Sci USA*. 1990;87:4453–7.
34. Unger J, McNeill TH, Moxley RT, 3rd, White M, Moss A, Livingston JN. Distribution of insulin receptor-like immunoreactivity in the rat forebrain. *Neuroscience*. 1989;31:143–57.
35. Frolich L, Blum-Degen D, Bernstein HG, *et al*. Brain insulin and insulin receptors in aging and sporadic Alzheimer's disease. *J Neural Transm (Vienna)*. 1998;105:423–38.
36. Doré S, Kar S, Rowe W, Quirion R. Distribution and levels of [125I]IGF-I, [125I]IGF-II and [125I]insulin receptor binding sites in the hippocampus of aged memory-unimpaired and -impaired rats. *Neuroscience*. 1997;80:1033–40.
37. Kar S, Chabot JG, Quirion R. Quantitative autoradiographic localization of [125I]insulin-like growth factor I, [125I]insulin-like growth factor II, and [125I]insulin receptor binding sites in developing and adult rat brain. *J Comp Neurol*. 1993;333: 375–97.
38. Baskin DG, Brewitt B, Davidson DA, *et al*. Quantitative autoradiographic evidence for insulin receptors in the choroid plexus of the rat brain. *Diabetes*. 1986;35:246–9.
39. Marks JL, Porte D, Jr., Stahl WL, Baskin DG. Localization of insulin receptor mRNA in rat brain by *in situ* hybridization. *Endocrinology*. 1990;127:3234–6.
40. Vanlandewijck M, He L, Mae MA, *et al*. A molecular atlas of cell types and zonation in the brain vasculature. *Nature*. 2018;554: 475–80.
41. Yang AC, Vest RT, Kern F, *et al*. A human brain vascular atlas reveals diverse mediators of Alzheimer's risk. *Nature*. 2022; 603:885–92.
42. Zhang W, Liu QY, Haqqani AS, *et al*. Differential expression of receptors mediating receptor-mediated transcytosis (RMT) in brain microvessels, brain parenchyma and peripheral tissues of the mouse and the human. *Fluids Barriers CNS*. 2020;17:47.
43. Gali CC, Fanaee-Danesh E, Zandl-Lang M, *et al*. Amyloid-beta impairs insulin signaling by accelerating autophagy-lysosomal degradation of LRP-1 and IR-β in blood-brain barrier endothelial cells in vitro and in 3XTg-AD mice. *Mol Cell Neurosci*. 2019;99:103390.
44. Rhea EM, Banks WA. Role of the blood-brain barrier in central nervous system insulin resistance. *Front Neurosci*. 2019;13: 521.

45. Baura GD, Foster DM, Porte D, Jr., *et al*. Saturable transport of insulin from plasma into the central nervous system of dogs in vivo. A mechanism for regulated insulin delivery to the brain. *J Clin Invest*. 1993;92:1824–30.
46. Duffy KR, Pardridge WM. Blood-brain barrier transcytosis of insulin in developing rabbits. *Brain Res*. 1987;420:32–8.
47. Banks WA, Kastin AJ. Differential permeability of the blood-brain barrier to two pancreatic peptides: Insulin and amylin. *Peptides*. 1998;19:883–9.
48. Gray SM, Aylor KW, Barrett EJ. Unravelling the regulation of insulin transport across the brain endothelial cell. *Diabetologia*. 2017;60:1512–21.
49. Woods SC, Seeley RJ, Baskin DG, Schwartz MW. Insulin and the blood-brain barrier. *Curr Pharm Des*. 2003;9:795–800.
50. Rhea EM, Rask-Madsen C, Banks WA. Insulin transport across the blood-brain barrier can occur independently of the insulin receptor. *J Physiol*. 2018;596:4753–65.
51. Hersom M, Helms HC, Schmalz C, Pedersen TA, Buckley ST, Brodin B. The insulin receptor is expressed and functional in cultured blood-brain barrier endothelial cells but does not mediate insulin entry from blood to brain. *Am J Physiol Endocrinol Metab*. 2018;315:E531–42.
52. Gray SM, Barrett EJ. Insulin transport into the brain. *Am J Physiol Cell Physiol*. 2018;315:C125–36.
53. Bennett DA, Buchman AS, Boyle PA, Barnes LL, Wilson RS, Schneider JA. Religious Orders Study and rush memory and aging project. *J Alzheimers Dis*. 2018;64(s1):S161–89.
54. Bourassa P, Tremblay C, Schneider JA, Bennett DA, Calon F. Brain mural cell loss in the parietal cortex in Alzheimer's disease correlates with cognitive decline and TDP-43 pathology. *Neuropathol Appl Neurobiol*. 2020;46:458–77.
55. Bourassa P, Tremblay C, Schneider JA, Bennett DA, Calon F. Beta-amyloid pathology in human brain microvessel extracts from the parietal cortex: Relation with cerebral amyloid angiopathy and Alzheimer's disease. *Acta Neuropathol*. 2019;137:801–23.
56. Bennett DA, Schneider JA, Aggarwal NT, *et al*. Decision rules guiding the clinical diagnosis of Alzheimer's disease in two community-based cohort studies compared to standard practice in a clinic-based cohort study. *Neuroepidemiology*. 2006;27:169–76.
57. Wilson RS, Beckett LA, Barnes LL, *et al*. Individual differences in rates of change in cognitive abilities of older persons. *Psychol Aging*. 2002;17:179–93.
58. Bennett DA, Schneider JA, Arvanitakis Z, *et al*. Neuropathology of older persons without cognitive impairment from two community-based studies. *Neurology*. 2006;66:1837–44.
59. Bennett DA, Wilson RS, Schneider JA, *et al*. Natural history of mild cognitive impairment in older persons. *Neurology*. 2002;59:198–205.
60. Arvanitakis Z, Grodstein F, Bienias JL, *et al*. Relation of NSAIDs to incident AD, change in cognitive function, and AD pathology. *Neurology*. 2008;70:2219–25.
61. Arvanitakis Z, Schneider JA, Wilson RS, *et al*. Statins, incident Alzheimer disease, change in cognitive function, and neuropathology. *Neurology*. 2008;70:1795–802.
62. Montine TJ, Phelps CH, Beach TG, *et al*. National institute on aging-Alzheimer's association guidelines for the neuropathologic assessment of Alzheimer's disease: A practical approach. *Acta Neuropathol*. 2012;123:1–11.
63. Thal DR, Rüb U, Orantes M, Braak H. Phases of A beta-deposition in the human brain and its relevance for the development of AD. *Neurology*. 2002;58:1791–800.
64. Braak H, Braak E. Neuropathological stageing of Alzheimer-related changes. *Acta Neuropathol*. 1991;82:239–59.
65. Mirra SS, Heyman A, McKeel D, *et al*. The consortium to establish a registry for Alzheimer's disease (CERAD). part II. Standardization of the neuropathologic assessment of Alzheimer's disease. *Neurology*. 1991;41:479–86.
66. Bennett DA, Wilson RS, Schneider JA, *et al*. Apolipoprotein E epsilon4 allele, AD pathology, and the clinical expression of Alzheimer's disease. *Neurology*. 2003;60:246–52.
67. Tremblay C, Francois A, Delay C, *et al*. Association of neuropathological markers in the parietal cortex with antemortem cognitive function in persons with mild cognitive impairment and Alzheimer disease. *J Neuropathol Exp Neurol*. 2017;76:70–88.
68. Tremblay C, Pilote M, Phivilay A, Emond V, Bennett DA, Calon F. Biochemical characterization of Abeta and tau pathologies in mild cognitive impairment and Alzheimer's disease. *J Alzheimers Dis*. 2007;12:377–90.
69. Oddo S, Caccamo A, Shepherd JD, *et al*. Triple-transgenic model of Alzheimer's disease with plaques and tangles: Intracellular Abeta and synaptic dysfunction. *Neuron*. 2003;39:409–21.
70. Julien C, Tremblay C, Phivilay A, *et al*. High-fat diet aggravates amyloid-beta and tau pathologies in the 3xTg-AD mouse model. *Neurobiol Aging*. 2010;31:1516–31.
71. Belfiore R, Rodin A, Ferreira E, *et al*. Temporal and regional progression of Alzheimer's disease-like pathology in 3xTg-AD mice. *Aging Cell*. 2019;18:e12873.
72. Vandal M, White PJ, Tournissac M, *et al*. Impaired thermoregulation and beneficial effects of thermoneutrality in the 3xTg-AD model of Alzheimer's disease. *Neurobiol Aging*. 2016;43:47–57.
73. Vandal M, White PJ, Chevrier G, *et al*. Age-dependent impairment of glucose tolerance in the 3xTg-AD mouse model of Alzheimer's disease. *FASEB J*. 2015;29:4273–84.
74. Do TM, Dodacki A, Alata W, *et al*. Age-dependent regulation of the blood-brain barrier influx/efflux equilibrium of amyloid-beta peptide in a mouse model of Alzheimer's disease (3xTg-AD). *J Alzheimers Dis*. 2015;49:287–300.
75. Stargardt A, Gillis J, Kamphuis W, *et al*. Reduced amyloid-β degradation in early Alzheimer's disease but not in the APPswePS1dE9 and 3xTg-AD mouse models. *Aging Cell*. 2013;12:499–507.
76. Bosoi CR, Vandal M, Tournissac M, *et al*. High-fat diet modulates hepatic amyloid β and cerebrosterol metabolism in the triple transgenic mouse model of Alzheimer's disease. *Hepatol Commun*. 2021;5:446–60.
77. Barron AM, Rosario ER, Elteriefi R, Pike CJ. Sex-specific effects of high fat diet on indices of metabolic syndrome in 3xTg-AD mice: Implications for Alzheimer's disease. *PLoS ONE*. 2013;8:e78554.
78. Robison LS, Gannon OJ, Thomas MA, *et al*. Role of sex and high-fat diet in metabolic and hypothalamic disturbances in the 3xTg-AD mouse model of Alzheimer's disease. *J Neuroinflammation*. 2020;17:285.
79. Chen Y, Zhao Y, Dai CL, *et al*. Intranasal insulin restores insulin signaling, increases synaptic proteins, and reduces Abeta level and microglia activation in the brains of 3xTg-AD mice. *Exp Neurol*. 2014;261:610–19.
80. Traversy MT, Vandal M, Tremblay C, *et al*. Altered cerebral insulin response in transgenic mice expressing the epsilon-4 allele of the human apolipoprotein E gene. *Psychoneuroendocrinology*. 2017;77:203–10.
81. Do TM, Alata W, Dodacki A, *et al*. Altered cerebral vascular volumes and solute transport at the blood-brain barriers of two

transgenic mouse models of Alzheimer's disease. *Neuropharmacology*. 2014;81:311–7.
82. Escribano O, Guillén C, Nevado C, Gómez-Hernández A, Kahn CR, Benito M. Beta-cell hyperplasia induced by hepatic insulin resistance: Role of a liver-pancreas endocrine axis through insulin receptor A isoform. *Diabetes*. 2009;58:820–8.
83. Kaminska D, Hämäläinen M, Cederberg H, *et al*. Adipose tissue INSR splicing in humans associates with fasting insulin level and is regulated by weight loss. *Diabetologia*. 2014;57: 347–51.
84. Besic V, Shi H, Stubbs RS, Hayes MT. Aberrant liver insulin receptor isoform A expression normalises with remission of type 2 diabetes after gastric bypass surgery. *PLoS ONE*. 2015;10:e0119270.
85. Chettouh H, Fartoux L, Aoudjehane L, *et al*. Mitogenic insulin receptor-A is overexpressed in human hepatocellular carcinoma due to EGFR-mediated dysregulation of RNA splicing factors. *Cancer Res*. 2013;73:3974–86.
86. Deane R, Wu Z, Sagare A, *et al*. LRP/Amyloid beta-peptide interaction mediates differential brain efflux of Abeta isoforms. *Neuron*. 2004;43:333–44.
87. Storck SE, Meister S, Nahrath J, *et al*. Endothelial LRP1 transports amyloid-beta(1-42) across the blood-brain barrier. *J Clin Invest*. 2016;126:123–36.
88. Flatt PR, Bailey CJ. Abnormal plasma glucose and insulin responses in heterozygous lean (ob/+) mice. *Diabetologia*. 1981; 20:573–7.
89. Ahrén B, Månsson S, Gingerich RL, Havel PJ. Regulation of plasma leptin in mice: Influence of age, high-fat diet, and fasting. *Am J Physiol*. 1997;273(1 Pt 2):R113–20.
90. Williams IM, Valenzuela FA, Kahl SD, *et al*. Insulin exits skeletal muscle capillaries by fluid-phase transport. *J Clin Invest*. 2018;128:699–714.
91. Meakin PJ, Mezzapesa A, Benabou E, *et al*. The beta secretase BACE1 regulates the expression of insulin receptor in the liver. *Nat Commun*. 2018;9:1306.
92. Bao H, Liu Y, Zhang M, *et al*. Increased beta-site APP cleaving enzyme 1-mediated insulin receptor cleavage in type 2 diabetes mellitus with cognitive impairment. *Alzheimers Dement*. 2021;17:1097–108.
93. Baskin DG, Porte D, Jr., Guest K, Dorsa DM. Regional concentrations of insulin in the rat brain. *Endocrinology*. 1983;112: 898–903.
94. Cai W, Xue C, Sakaguchi M, *et al*. Insulin regulates astrocyte gliotransmission and modulates behavior. *J Clin Invest*. 2018; 128:2914–26.
95. García-Cáceres C, Quarta C, Varela L, *et al*. Astrocytic insulin signaling couples brain glucose uptake with nutrient availability. *Cell*. 2016;166:867–80.
96. Schubert M, Gautam D, Surjo D, *et al*. Role for neuronal insulin resistance in neurodegenerative diseases. *Proc Natl Acad Sci USA*. 2004;101:3100–5.
97. Garwood CJ, Ratcliffe LE, Morgan SV, *et al*. Insulin and IGF1 signalling pathways in human astrocytes in vitro and in vivo; characterisation, subcellular localisation and modulation of the receptors. *Mol Brain*. 2015;8:51.
98. Gralle M, Labrecque S, Salesse C, De Koninck P. Spatial dynamics of the insulin receptor in living neurons. *J Neurochem*. 2021; 156:88–105.
99. Jin Z, Jin Y, Kumar-Mendu S, Degerman E, Groop L, Birnir B. Insulin reduces neuronal excitability by turning on GABA(A) channels that generate tonic current. *PLoS ONE*. 2011;6:e16188.
100. Sartorius T, Peter A, Heni M, *et al*. The brain response to peripheral insulin declines with age: A contribution of the blood-brain barrier? *PLoS ONE*. 2015;10:e0126804.
101. Hooshmand B, Rusanen M, Ngandu T, *et al*. Serum insulin and cognitive performance in older adults: A longitudinal study. *Am J Med*. 2019;132:367–73.
102. Li H, Zhu H, Wallack M, *et al*. Age and its association with low insulin and high amyloid-β peptides in blood. *J Alzheimers Dis*. 2015;49:129–37.
103. Zhao WQ, Chen H, Quon MJ, Alkon DL. Insulin and the insulin receptor in experimental models of learning and memory. *Eur J Pharmacol*. 2004;490:71–81.
104. Banks WA, Jaspan JB, Kastin AJ. Effect of diabetes mellitus on the permeability of the blood-brain barrier to insulin. *Peptides*. 1997;18:1577–84.
105. Urayama A, Banks WA. Starvation and triglycerides reverse the obesity-induced impairment of insulin transport at the blood-brain barrier. *Endocrinology*. 2008;149:3592–7.
106. Banks WA, Farr SA, Morley JE. Permeability of the blood-brain barrier to albumin and insulin in the young and aged SAMP8 mouse. *J Gerontol A Biol Sci Med Sci*. 2000;55:B601–6.
107. Vella V, Milluzzo A, Scalisi NM, Vigneri P, Sciacca L. Insulin receptor isoforms in cancer. *Int J Mol Sci*. 2018;19:3615.
108. Escribano O, Beneit N, Rubio-Longás C, López-Pastor AR, Gómez-Hernández A. The role of insulin receptor isoforms in diabetes and its metabolic and vascular complications. *J Diabetes Res*. 2017;2017:1–12.
109. Scalia P, Giordano A, Martini C, Williams SJ. Isoform- and paralog-switching in IR-signaling: When diabetes opens the gates to cancer. *Biomolecules*. 2020;10:1617.
110. Pandini G, Frasca F, Mineo R, Sciacca L, Vigneri R, Belfiore A. Insulin/insulin-like growth factor I hybrid receptors have different biological characteristics depending on the insulin receptor isoform involved. *J Biol Chem*. 2002;277:39684–95.
111. Benyoucef S, Surinya KH, Hadaschik D, Siddle K. Characterization of insulin/IGF hybrid receptors: Contributions of the insulin receptor L2 and Fn1 domains and the alternatively spliced exon 11 sequence to ligand binding and receptor activation. *Biochem J*. 2007; 403:603–13.
112. Slaaby R, Schäffer L, Lautrup-Larsen I, *et al*. Hybrid receptors formed by insulin receptor (IR) and insulin-like growth factor I receptor (IGF-IR) have low insulin and high IGF-1 affinity irrespective of the IR splice variant. *J Biol Chem*. 2006;281:25869–74.
113. Arvanitakis Z, Capuano AW, Wang HY, *et al*. Brain insulin signaling and cerebrovascular disease in human postmortem brain. *Acta Neuropathol Commun*. 2021;9:71.
114. Velazquez R, Tran A, Ishimwe E, *et al*. Central insulin dysregulation and energy dyshomeostasis in two mouse models of Alzheimer's disease. *Neurobiol Aging*. 2017;58:1–13.
115. Kappeler L, De Magalhaes Filho C, Dupont J, *et al*. Brain IGF-1 receptors control mammalian growth and lifespan through a neuroendocrine mechanism. *PLoS Biol*. 2008;6:e254.
116. Torres-Aleman I. Targeting insulin-like growth factor-1 to treat Alzheimer's disease. *Expert Opin Ther Targets*. 2007;11: 1535–42.
117. Steen E, Terry BM, Rivera EJ, *et al*. Impaired insulin and insulin-like growth factor expression and signaling mechanisms in Alzheimer's disease – Is this type 3 diabetes? *J Alzheimers Dis*. 2005;7:63–80.
118. Rivera EJ, Goldin A, Fulmer N, Tavares R, Wands JR, de la Monte SM. Insulin and insulin-like growth factor expression and function deteriorate with progression of Alzheimer's disease: Link to brain reductions in acetylcholine. *J Alzheimers Dis*. 2005;8:247–68.
119. de la Monte SM. Insulin resistance and neurodegeneration: Progress towards the development of new therapeutics for Alzheimer's disease. *Drugs*. 2017;77:47–65.

120. Gualco E, Wang JY, Del Valle L, *et al*. IGF-IR in neuroprotection and brain tumors. *Front Biosci (Landmark Ed)*. 2009;14:352–75.
121. Rosenzweig SA. The continuing evolution of insulin-like growth factor signaling. *F1000Res*. 2020;9:205.
122. Denley A, Cosgrove LJ, Booker GW, Wallace JC, Forbes BE. Molecular interactions of the IGF system. *Cytokine Growth Factor Rev*. 2005;16:421–39.
123. Macauley SL, Stanley M, Caesar EE, *et al*. Hyperglycemia modulates extracellular amyloid-β concentrations and neuronal activity in vivo. *J Clin Invest*. 2015;125:2463–7.
124. Miners JS, Van Helmond Z, Chalmers K, Wilcock G, Love S, Kehoe PG. Decreased expression and activity of neprilysin in Alzheimer disease are associated with cerebral amyloid angiopathy. *J Neuropathol Exp Neurol*. 2006;65:1012–21.
125. Farris W, Mansourian S, Chang Y, *et al*. Insulin-degrading enzyme regulates the levels of insulin, amyloid beta-protein, and the beta-amyloid precursor protein intracellular domain *in vivo*. *Proc Natl Acad Sci USA*. 2003;100:4162–7.
126. Kurochkin IV, Goto S. Alzheimer's beta-amyloid peptide specifically interacts with and is degraded by insulin degrading enzyme. *FEBS Lett*. 1994;345:33–7.
127. Hladky SB, Barrand MA. Elimination of substances from the brain parenchyma: efflux via perivascular pathways and via the blood-brain barrier. *Fluids Barriers CNS*. 2018;15:30.
128. Storck SE, Hartz AMS, Pietrzik CU. The blood-brain barrier in Alzheimer's disease. *Handb Exp Pharmacol*. 2022. https://doi.org/10.1007/164_2020_418
129. Xie L, Helmerhorst E, Taddei K, Plewright B, Van Bronswijk W, Martins R. Alzheimer's beta-amyloid peptides compete for insulin binding to the insulin receptor. *J Neurosci*. 2002;22:RC221.
130. Vassar R, Bennett BD, Babu-Khan S, *et al*. Beta-secretase cleavage of Alzheimer's amyloid precursor protein by the transmembrane aspartic protease BACE. *Science*. 1999;286:735–41.
131. Stockley JH, O'Neill C. The proteins BACE1 and BACE2 and beta-secretase activity in normal and Alzheimer's disease brain. *Biochem Soc Trans*. 2007;35(Pt 3):574–6.
132. Li R, Lindholm K, Yang LB, *et al*. Amyloid beta peptide load is correlated with increased beta-secretase activity in sporadic Alzheimer's disease patients. *Proc Natl Acad Sci USA*. 2004;101:3632–3637.
133. Fukumoto H, Cheung BS, Hyman BT, Irizarry MC. Beta-secretase protein and activity are increased in the neocortex in Alzheimer disease. *Arch Neurol*. 2002;59:1381–9.
134. Kwart D, Gregg A, Scheckel C, *et al*. A large panel of isogenic APP and PSEN1 mutant human iPSC neurons reveals shared endosomal abnormalities mediated by APP β-CTFs, not Aβ. *Neuron*. 2019;104:256–70.e5.
135. Chen Z, Oliveira SDS, Zimnicka AM, *et al*. Reciprocal regulation of eNOS and caveolin-1 functions in endothelial cells. *Mol Biol Cell*. 2018;29:1190–202.
136. Haddad D, Al Madhoun A, Nizam R, Al-Mulla F. Role of caveolin-1 in diabetes and its complications. *Oxid Med Cell Longev*. 2020;2020:1–20.
137. Taylor NA, Van De Ven WJ, Creemers JW. Curbing activation: Proprotein convertases in homeostasis and pathology. *Faseb J*. 2003;17:1215–27.
138. Kim SH, Wang R, Gordon DJ, *et al*. Furin mediates enhanced production of fibrillogenic ABri peptides in familial British dementia. *Nat Neurosci*. 1999;2:984–88.
139. He L, Vanlandewijck M, Mäe MA, *et al*. Single-cell RNA sequencing of mouse brain and lung vascular and vessel-associated cell types. *Sci Data*. 2018;5:180160.
140. Hampel H, Vassar R, De Strooper B, *et al*. The β-secretase BACE1 in Alzheimer's disease. *Biol Psychiatry*. 2021;89:745–56.
141. Devraj K, Poznanovic S, Spahn C, *et al*. BACE-1 is expressed in the blood-brain barrier endothelium and is upregulated in a murine model of Alzheimer's disease. *J Cereb Blood Flow Metab*. 2016;36:1281–94.
142. Yuasa T, Amo-Shiinoki K, Ishikura S, *et al*. Sequential cleavage of insulin receptor by calpain 2 and γ-secretase impairs insulin signalling. *Diabetologia*. 2016;59:2711–21.
143. Gaborit B, Govers R, Altié A, Brunel JM, Morange P, Peiretti F. The aminosterol claramine inhibits β-secretase 1-mediated insulin receptor cleavage. *J Biol Chem*. 2021;297:100818.
144. Soluble Insulin Receptor Study Group. Soluble insulin receptor ectodomain is elevated in the plasma of patients with diabetes. *Diabetes*. 2007;56:2028–35.
145. Shen Y, Wang H, Sun Q, *et al*. Increased plasma beta-secretase 1 may predict conversion to Alzheimer's disease dementia in individuals with mild cognitive impairment. *Biol Psychiatry*. 2018;83:447–55.